International Conference on Adaptive Modeling and Simulation
ADMOS 2023
F.Larsson and P.Díez

MESH- AND MODEL ADAPTIVITY FOR ELASTO-PLASTIC MEAN-FIELD AND FULL-FIELD HOMOGENIZATION BASED ON DOWNWIND AND UPWIND APPROXIMATIONS

A. TCHOMGUE SIMEU*, R. MAHNKEN †

* Chair of Engineering Mechanics (LTM)
University of Paderborn
Warburger Str. 100, 33098 Paderborn, Germany
e-mail: simeu@ltm.upb.de, web page: https://mb.uni-paderborn.de/ltm

† e-mail: mahnken@ltm.upb.de

Key words: Adaptive Modeling, Meshing and Remeshing, Goal oriented Adaptivity

Summary. Materials such as composites are heterogeneous at the micro-scale, where several constituents with different material properties can be distinguished like elastic inclusions and the elasto-plastic matrix with isotropic hardening. One has to deal with these heterogeneities on the micro-scale and then perform a scale transition to obtain the overall behavior on the macro-scale, which is often referred to as homogenization. The present contribution deals with the combination of numerically inexpensive mean-field and numerically expensive full-field homogenization methods in elasto-plasticity coupled to adaptive finite element method (FEM) which takes into account error generation and error transport at each time step on the macro-scale. The proposed adaptive procedure is driven by a goal-oriented a posteriori error estimator based on duality techniques. The main difficulty of duality techniques in the literature is that the backwards-in-time algorithm has a high demand on memory capacity since additional memory is required to store the primary solutions computed over all time steps. To this end, several downwind and upwind approximations are introduced for an elasto-plastic primal problem by means of jump terms [1]. Therefore, from a computational point of view, the forwards-in-time duality problem is very attractive. A numerical example illustrates the effectiveness of the proposed adaptive approach based on forwards-in-time method in comparison to backwards-in-time method.

1 INTRODUCTION

In this work, a goal oriented framework considers error generation and error transport at each time step. The discretization errors generated in the current time step are transported into the next time step. This error accumulation over time is described either with a forwards-in-time method or a backwards-in-time method by resolving a dual problem. Furthermore, the primal problem is resolved with jump terms for time integration by temporally constant test and trial functions applied to the constitutive equations of von Mises elasto-plasticity. By means of the jump terms, the primal problem is solved either with a downwind approximation or an upwind approximation leading to eight different approximations not only for solution of primal problem, but also for problems dual to primal problem. These approximations require the Prandtl-Reuss tensor and a strain tensor or a stress tensor at each time step.

2 A TWO-SCALE PROBLEM

2.1 Initial boundary value problem of the micro-structure and macro-structure

The macro initial value boundary problem (IVBP) $\overline{P}$ and the micro problem P read

$$\overline{P}\colon \begin{cases} 1.\ \mathrm{Div}(\overline{\boldsymbol{\sigma}}) + \overline{\boldsymbol{b}} = \boldsymbol{0}, & \text{in } \overline{\Omega}\times I \\ 2.\ \overline{\boldsymbol{\varepsilon}}(\overline{\boldsymbol{u}}) = \nabla^{\mathrm{sym}}\overline{\boldsymbol{u}}, & \text{in } \overline{\Omega}\times I \\ 3.\ \dot{\overline{\boldsymbol{\sigma}}} = \overline{\mathbb{P}}(\overline{\boldsymbol{x}})\dot{\overline{\boldsymbol{\varepsilon}}}(\overline{\boldsymbol{x}}), & \text{in } \overline{\Omega}\times I \\ 4.\ \overline{\boldsymbol{\sigma}}\boldsymbol{N} = \overline{\boldsymbol{t}}, & \text{on } \overline{\Gamma}_t \\ 5.\ \overline{\boldsymbol{u}} = \overline{\boldsymbol{u}}^*, & \text{on } \overline{\Gamma}_u \\ 6.\ \overline{\boldsymbol{u}} = \overline{\boldsymbol{u}}^0(\overline{\boldsymbol{x}}), & \text{in } \overline{\Omega}\times\{t_0\} \end{cases}, \quad P\colon \begin{cases} 7.\ \mathrm{Div}(\boldsymbol{\sigma}(\boldsymbol{x})) = \boldsymbol{0}, & \text{in } \Omega\times I \\ 8.\ \boldsymbol{\varepsilon}(\boldsymbol{u}) = \nabla^{\mathrm{sym}}\boldsymbol{u}, & \text{in } \Omega\times I \\ 9.\ \dot{\boldsymbol{\sigma}} = \mathbb{P}(\boldsymbol{x})\dot{\boldsymbol{\varepsilon}}(\boldsymbol{x}), & \text{in } \Omega\times I \\ 10.\ \boldsymbol{u} = \boldsymbol{u}^0(\boldsymbol{x}), & \text{in } \Omega\times\{t_0\} \\ 11.\ +\ \text{boundary conditions} \end{cases}, \quad (1)$$

respectively. Eqs. (1.1) and (1.7) are the macro and micro equilibrium problems. $\overline{\boldsymbol{\sigma}}$, $\boldsymbol{\sigma}$ and $\overline{\boldsymbol{b}}$ denote the macro and micro stresses tensor and the body force, respectively. Eqs. (1.2) and (1.8) prescribe the small strain tensor as a symmetric gradient of the displacement vector on the macro and micro scale, respectively. The stress rate $\dot{\overline{\boldsymbol{\sigma}}}(\overline{\boldsymbol{x}})$ is related to the strain rate $\dot{\overline{\boldsymbol{\varepsilon}}}(\overline{\boldsymbol{x}})$ with the effective material tangent $\overline{\mathbb{P}}(\overline{\boldsymbol{x}})$ in Eq. (1.3) [2]. Eq. (1.9) is the constitutive relation in rate form. Eq. (1.4) and Eq. (1.5) represent the Neumann boundary condition $\overline{\Gamma}_t$ and the Dirichlet boundary condition $\overline{\Gamma}_u$, respectively, where $\overline{\boldsymbol{t}}$ is the tractions imposed on $\overline{\Gamma}_t$ and $\overline{\boldsymbol{u}}^*$ indicates the prescribed displacements on $\overline{\Gamma}_u$. The properties $\overline{\Gamma}_u \bigcup \overline{\Gamma}_t = \overline{\Gamma}$ and $\overline{\Gamma}_u \bigcap \overline{\Gamma}_t = \emptyset$ are valid. Periodic boundary conditions hold on the micro-scale [3]. Eqs. (1.6), (1.10) and (1.11) prescribe initial conditions. The scale transition is established by means of $\overline{\boldsymbol{\varepsilon}} = \langle\boldsymbol{\varepsilon}(\boldsymbol{x})\rangle$ and $\overline{\boldsymbol{\sigma}} = \langle\boldsymbol{\sigma}(\boldsymbol{x})\rangle$ and by the Hill-Mandel condition [4]

$$\langle\dot{\boldsymbol{\sigma}}\colon\boldsymbol{\varepsilon}\rangle = \langle\dot{\boldsymbol{\sigma}}\rangle\colon\langle\boldsymbol{\varepsilon}\rangle = \dot{\overline{\boldsymbol{\sigma}}}\colon\overline{\boldsymbol{\varepsilon}}, \qquad \text{where} \qquad \langle\bullet\rangle = \frac{1}{|\,\Omega\,|}\int_\Omega \bullet dv. \qquad (2)$$

2.2 Weak form for the macro-primal problem and the dual problem

To solve the macro-problem $\overline{P}$ with FEM we introduce a weak form and integrate over the time interval I to obtain a global weak form, which is equivalent to the formulations

for the problem $\overline{P}$ in Eq.(1):

$$\begin{aligned}
&\overline{P}_w : \text{Find } \overline{\boldsymbol{u}} \in \overline{\mathcal{V}}, \text{ such that} \\
&\overline{\rho}(\overline{\boldsymbol{u}}, \delta\overline{\boldsymbol{u}}) = \overline{F}(\delta\overline{\boldsymbol{u}}) - \overline{B}(\overline{\boldsymbol{u}}; \delta\overline{\boldsymbol{u}}) \quad \forall \delta\overline{\boldsymbol{u}} \in \overline{\mathcal{V}}_\delta = 0, \qquad \text{where} && \text{(3a)} \\
&\overline{F}(\delta\overline{\boldsymbol{u}}) := \int_I \left(\left\langle \dot{\overline{\boldsymbol{b}}} \cdot \delta\overline{\boldsymbol{u}} \right\rangle_{\overline{\Omega}} \right) dt + \int_I \left\langle \dot{\overline{\boldsymbol{t}}} \cdot \delta\overline{\boldsymbol{u}} \right\rangle_{\overline{\Gamma}_t} dt + \left\langle \overline{\boldsymbol{u}}^0 : \delta\overline{\boldsymbol{u}}(t_0) \right\rangle , && \text{(3b)} \\
&\overline{B}(\overline{\boldsymbol{u}}; \delta\overline{\boldsymbol{u}}) := \int_I < \dot{\overline{\boldsymbol{\varepsilon}}}(\overline{\boldsymbol{u}}) : \overline{\mathbb{P}}^{\mathrm{T}}(\overline{\boldsymbol{u}}) : \delta\overline{\boldsymbol{\varepsilon}}(\delta\overline{\boldsymbol{u}}) > dt + \langle \overline{\boldsymbol{u}}(t_0) : \delta\overline{\boldsymbol{u}}(t_0) \rangle . && \text{(3c)}
\end{aligned}$$

The upper index T denotes the transpose of the respective tensor. $\overline{F}(\cdot)$ is a linear form, while $\overline{B}(\cdot;\cdot)$ is a bilinear form. Note, that the weak form (3) considers the initial condition Eq. (1.6). The *strain rate bilinear form* $\overline{B}^{\varepsilon}(\overline{\boldsymbol{u}}; \delta\overline{\boldsymbol{u}})$ and the *stress rate bilinear form* $\overline{B}^{\sigma}(\overline{\boldsymbol{u}}; \delta\overline{\boldsymbol{u}})$ are distinguished as

$$\overline{B}(\overline{\boldsymbol{u}}; \delta\overline{\boldsymbol{u}}) : \begin{cases} 1. \quad \overline{B}^{\varepsilon}(\overline{\boldsymbol{u}}; \delta\overline{\boldsymbol{u}}) \;\; := \int_I < \dot{\overline{\boldsymbol{\varepsilon}}}(\overline{\boldsymbol{u}}) : \delta\overline{\boldsymbol{\sigma}}(\overline{\boldsymbol{u}}, \delta\overline{\boldsymbol{u}}) > dt + \langle \overline{\boldsymbol{u}}(t_0) : \delta\overline{\boldsymbol{u}}(t_0) \rangle , \\ 2. \quad \overline{B}^{\sigma}(\overline{\boldsymbol{u}}; \delta\overline{\boldsymbol{u}}) \;\; := \int_I < \dot{\overline{\boldsymbol{\sigma}}}(\overline{\boldsymbol{u}}) : \delta\overline{\boldsymbol{\varepsilon}}(\delta\overline{\boldsymbol{u}}) > dt + \langle \overline{\boldsymbol{u}}(t_0) : \delta\overline{\boldsymbol{u}}(t_0) \rangle , \end{cases} \tag{4}$$

where the hybrid-test stress tensor $\delta\overline{\boldsymbol{\sigma}}(\overline{\boldsymbol{u}}, \delta\overline{\boldsymbol{u}})$ is defined as $\delta\overline{\boldsymbol{\sigma}}(\overline{\boldsymbol{u}}, \delta\overline{\boldsymbol{u}}) := \overline{\mathbb{P}}^{\mathrm{T}}(\overline{\boldsymbol{u}}) : \delta\overline{\boldsymbol{\varepsilon}}(\delta\overline{\boldsymbol{u}})$. A quantity of interest and its corresponding total error are written as the following general forms

$$1.\; Q(\overline{\boldsymbol{u}}) := \int_I Q_1(\overline{\boldsymbol{u}}) dt + Q_2(\overline{\boldsymbol{u}}_T) , \qquad 2.\; E(\overline{\boldsymbol{u}}, \overline{\boldsymbol{u}}^{\mathrm{r}}) := Q(\overline{\boldsymbol{u}}) - Q(\overline{\boldsymbol{u}}^{\mathrm{r}}) , \tag{5}$$

where Q_1 is a time integral part and Q_2 is a part at the final time T [5]. For the exact model (3a) to be practically solved, we need to introduce an additional surrogate model $\tilde{\overline{\varrho}}(\overline{\boldsymbol{u}}^{\mathrm{r}}; \delta\overline{\boldsymbol{u}}) = \tilde{\overline{F}}(\delta\overline{\boldsymbol{u}}) - \tilde{\overline{B}}(\overline{\boldsymbol{u}}^{\mathrm{r}}; \delta\overline{\boldsymbol{u}}) = 0$, $\forall \delta\overline{\boldsymbol{u}} \in \overline{\mathcal{V}}_\delta$ with its solution $\overline{\boldsymbol{u}}^{\mathrm{r}}$ as an approximation of the exact solution $\overline{\boldsymbol{u}}$. Due to discretization and model errors, generally, the functionals $\tilde{\overline{F}}(\delta\overline{\boldsymbol{u}})$ and $\tilde{\overline{B}}(\overline{\boldsymbol{u}}^{\mathrm{r}}; \delta\overline{\boldsymbol{u}})$ are approximations to the functionals $\overline{F}(\delta\overline{\boldsymbol{u}})$ and $\overline{B}(\overline{\boldsymbol{u}}; \delta\overline{\boldsymbol{u}})$ of the exact model (3a). Taking Eq. (5) into account, the following dual problem is defined

$$\begin{aligned}
&\overline{D}_w : \text{Find } \overline{\boldsymbol{z}} \in \overline{\mathcal{V}}, \text{ such that} \\
&\overline{\rho_z}(\overline{\boldsymbol{u}}^{\mathrm{r}}, \overline{\boldsymbol{z}}; \delta\overline{\boldsymbol{u}}) = \mathrm{D}_{\overline{\boldsymbol{u}}^{\mathrm{r}}} E(\overline{\boldsymbol{u}}, \overline{\boldsymbol{u}}^{\mathrm{r}}; \delta\overline{\boldsymbol{u}}) - \mathrm{D}_{\overline{\boldsymbol{u}}^{\mathrm{r}}} \tilde{\overline{B}}(\overline{\boldsymbol{u}}^{\mathrm{r}}; \overline{\boldsymbol{z}}, \delta\overline{\boldsymbol{u}}) = 0 \;\; \forall \; \delta\overline{\boldsymbol{u}} \in \overline{\mathcal{V}}_\delta, \quad \text{where} && \text{(6a)} \\
&\mathrm{D}_{\overline{\boldsymbol{u}}^{\mathrm{r}}} E(\overline{\boldsymbol{u}}, \overline{\boldsymbol{u}}^{\mathrm{r}}; \delta\overline{\boldsymbol{u}}) = \mathrm{D}_{\overline{\boldsymbol{u}}^{\mathrm{r}}} \int_{I_i} Q_1(\overline{\boldsymbol{u}}; \delta\overline{\boldsymbol{u}}) dt + \mathrm{D}_{\overline{\boldsymbol{u}}^{\mathrm{r}}} Q_2(\overline{\boldsymbol{u}}_T; \delta\overline{\boldsymbol{u}}_T) , && \text{(6b)} \\
&\mathrm{D}_{\overline{\boldsymbol{u}}^{\mathrm{r}}} \tilde{\overline{B}}(\overline{\boldsymbol{u}}^{\mathrm{r}}; \overline{\boldsymbol{z}}, \delta\overline{\boldsymbol{u}}) = \mathrm{D}_{\overline{\boldsymbol{u}}^{\mathrm{r}}} \int_{I_i} \tilde{\overline{B}}_i(\overline{\boldsymbol{u}}^{\mathrm{r}}; \overline{\boldsymbol{z}}, \delta\overline{\boldsymbol{u}}) - \langle \delta\overline{\boldsymbol{u}}^{\mathrm{r}}(t_0), \overline{\boldsymbol{z}}(t_0) \rangle . && \text{(6c)}
\end{aligned}$$

3 Time discretization of macro primal problem and dual problem

3.1 Upwind and downwind approximations

The variational local form (3a) can be used for discretization in space and in time. A general scheme is obtained by so-called $cG(s)dG(r)$ methods representing a space-time

discretization with continuous piecewiece-polynomials of degree s in space and discontinuous piecewiece-polynomials of degree r in time. Similarly, $cG(s)cG(r)$ denotes continuous piecewiece-polynomials in space and time, see e.g. [6]. We begin with a partition of the time interval $I = (t_0, T]$ as $t_0 < t_1 < ....t_i < .... < t_N = T$ and use the notations

$$\begin{aligned} &1. \quad \hat{I} = [t_0, T] = \{t_0\} \cup I = \{t_0\} \cup \textstyle\bigcup_{i=1}^{N} I_i, && 2. \quad I_i = (t_{i-1}, t_i], \\ &3. \quad \tau_i = t_i - t_{i-1}, \quad i = 1, .., N, && 4. \quad \tau = \{\max \tau_i\}_{i=1}^{N}. \end{aligned} \tag{7}$$

The bilinear form in Eq. (4) becomes $\overline{B}^{\alpha}(\overline{\boldsymbol{u}}, \delta\overline{\boldsymbol{u}}) = \sum_{i=1}^{N} \overline{B}_i^{\alpha}(\overline{\boldsymbol{u}}, \delta\overline{\boldsymbol{u}}) + \langle \overline{\boldsymbol{u}}(t_0) : \delta\overline{\boldsymbol{u}}(t_0)\rangle$ with $\alpha = \varepsilon, \sigma$. We select the semi-discrete spaces for test and trial functions, respectively,

$$\overline{\mathcal{V}}_{\delta}^{\,\mathrm{r}} = \left\{\delta\overline{\boldsymbol{u}}^{\mathrm{r}} : \overline{\mathcal{V}}_1^{\mathrm{r}} ... \otimes \overline{\mathcal{V}}_i^{\mathrm{r}} ... \otimes \overline{\mathcal{V}}_N^{\mathrm{r}}, \delta\overline{\boldsymbol{u}}^{\mathrm{r}}(t_0) \in \bar{V}\right\} \subset \overline{\mathcal{V}}_{\delta}, \tag{8a}$$

$$\overline{\mathcal{V}}^{\mathrm{r}} = \overline{\mathcal{V}}_{\delta}^{\,\mathrm{r}} \subset \overline{\mathcal{V}}, \quad \text{where} \tag{8b}$$

$$\overline{\mathcal{V}}_i^{\mathrm{r}} = \overline{\mathcal{V}}_{\delta i}^{\,\mathrm{r}} = \left\{\delta\overline{\boldsymbol{u}}_i^{\mathrm{r}} : (t_0, T] \to \bar{V};\, \delta\overline{\boldsymbol{u}}_i^{\mathrm{r}}|_{I_i} \in \mathcal{P}^{\mathrm{r}}(I_i, \bar{V}),\, \delta\overline{\boldsymbol{u}}_i^{\mathrm{r}}|_{\notin I_i} = 0\right\}. \tag{8c}$$

For the semi-discrete spaces $\overline{\mathcal{V}}_i^{\mathrm{r}}$ associated to each time interval I_i, $\mathcal{P}^{\mathrm{r}}(I_i, \bar{V})$ denotes the space of polynomials of a degree less than or equal to $r \in \mathbb{N}_0$ taking values in $\bar{V}$. Note that $\delta\overline{\boldsymbol{u}}^{\mathrm{r}}(t_0)$ has to be specified separately in Eq. (8a) since $t_0 \notin I_1$.

In the sequel, we give a brief description of the procedure to derive a discretized time stepping scheme. More details are given in [7]. Exemplarily we consider the stress rate bilinear form. Then, we use the discontinuous approximation $\overline{\boldsymbol{u}} \approx \overline{\boldsymbol{u}}^{\mathrm{r}}$ such that integrating by parts renders the integral over the subinterval I_i for the stress rate bilinear form

$$\overline{B}_i^{\sigma}(\overline{\boldsymbol{u}}^{\mathrm{r}}, \delta\overline{\boldsymbol{u}}^{\mathrm{r}}) = -\int_{I_i} \left\langle \overline{\boldsymbol{\sigma}}(\overline{\boldsymbol{u}}^{\mathrm{r}}) : \delta\dot{\overline{\boldsymbol{\varepsilon}}}(\delta\overline{\boldsymbol{u}}^{\mathrm{r}})\right\rangle dt + \left\langle \overline{\boldsymbol{\sigma}}_i^{-}(\overline{\boldsymbol{u}}^{\mathrm{r}}) : \delta\overline{\boldsymbol{\varepsilon}}(\delta\overline{\boldsymbol{u}}^{\mathrm{r}})_i^{-}\right\rangle - \left\langle \overline{\boldsymbol{\sigma}}_{i-1}^{+}(\overline{\boldsymbol{u}}^{\mathrm{r}}) : \delta\overline{\boldsymbol{\varepsilon}}(\delta\overline{\boldsymbol{u}}^{\mathrm{r}})_{i-1}^{+}\right\rangle. \tag{9}$$

Next, the jump of the displacement $\overline{\boldsymbol{u}}$ at each nodal point t_i is defined $\left[\overline{\boldsymbol{u}}\right]_i = \overline{\boldsymbol{u}}_i^{+} - \overline{\boldsymbol{u}}_i^{-}$ where $\overline{\boldsymbol{u}}_i^{+(-)} = \lim_{s\downarrow(\uparrow)0} \overline{\boldsymbol{u}}(t_i + s)$ [1]. A downwind approximation (d) and an upwind approximation (u) are applied on the stress tensor, the test strain tensor in Eq. (9). Then, the right hand side of Eq.(9) is integrated by parts again, we end up with four stresses rate bilinear form approximates. In total, there are eight different approximations for solution of the primal problem Eq. (3) and for the dual problem Eq. (6) taking the strain rate bilinear form into account.

To solve the primal problem with a downwind approximation, the initial value are $\overline{\boldsymbol{u}}_i^{-} = \overline{\boldsymbol{u}}_{i-1}^{+}$ at time t_{i-1}^{+} and $\overline{\boldsymbol{u}}_i^{+} =: \boldsymbol{U}_i$. Then, setting r = 0 in (8c) we choose trial and test functions as $\overline{\boldsymbol{u}}_i^{\mathrm{r}}(t) = \overline{\boldsymbol{u}}_{i-1}^{+} = \overline{\boldsymbol{u}}_i^{-} =: \boldsymbol{U}_{i-1} = \text{const}$ and $\delta\overline{\boldsymbol{u}}_i^{\mathrm{r}}(t) = \delta\overline{\boldsymbol{u}}_i^{\mathrm{r}} = \delta\overline{\boldsymbol{u}}_i^{-} =: \delta\boldsymbol{U}_i = \text{const}, \quad t \in I_i$. In view of Eqs. (1.2) and (1.3) we have $\dot{\overline{\boldsymbol{\varepsilon}}}(\overline{\boldsymbol{u}}_i^{\mathrm{r}}) = \nabla^{\mathrm{sym}}\dot{\overline{\boldsymbol{u}}}_i^{\mathrm{r}} = \boldsymbol{0}$, such that $\int_{I_i} \left\langle \dot{\overline{\boldsymbol{\sigma}}}(\overline{\boldsymbol{u}}_i^{\mathrm{r}}) \colon \delta\overline{\boldsymbol{\varepsilon}}(\delta\overline{\boldsymbol{u}}_i^{\mathrm{r}})\right\rangle dt = 0$. Then, a semi-discretized local problem of Eq. (3) is obtained as an explicit Euler forward time interaction scheme

$$\overline{\rho}_i(\boldsymbol{U}_i; \delta\boldsymbol{U}_i) = \overline{F}_i(\delta\boldsymbol{U}_i) - \langle(\overline{\boldsymbol{\sigma}}_i(\boldsymbol{U}_i) - \overline{\boldsymbol{\sigma}}_{i-1}(\boldsymbol{U}_{i-1})) : \delta\overline{\boldsymbol{\varepsilon}}_i(\delta\boldsymbol{U}_i)\rangle = 0\,, \tag{10a}$$

$$\overline{F}_i(\delta\overline{\boldsymbol{u}}_i^{\mathrm{r}}) \approx \left\langle \dot{\bar{\boldsymbol{b}}}(t_{i-1}) \cdot \delta\boldsymbol{U}_i \right\rangle_{\overline{\Omega}} \tau_i + < \dot{\bar{\boldsymbol{t}}}(t_{i-1}) \cdot \delta\boldsymbol{U}_i >_{\overline{\Gamma}_t} \tau_i\,, \quad \forall\ \delta\boldsymbol{U}_i \in \overline{\mathcal{V}}_{\delta i}^{\,\mathrm{r}}. \tag{10b}$$

In analogy to Eq. (10), an implicit Euler-backward time interaction scheme is obtained using the upwind approximation as

$$\overline{\rho}_i(\boldsymbol{U}_i;\delta\boldsymbol{U}_i) = \overline{F}_i(\delta\boldsymbol{U}_i) - \langle(\overline{\boldsymbol{\sigma}}_i(\boldsymbol{U}_i) - \overline{\boldsymbol{\sigma}}_{i-1}(\boldsymbol{U}_{i-1})) : \delta\overline{\boldsymbol{\varepsilon}}_i(\delta\boldsymbol{U}_i)\rangle = 0\,, \tag{11a}$$

$$\overline{F}_i(\delta\overline{\boldsymbol{u}}^{\mathrm{r}}_i) \approx \left\langle \dot{\bar{\boldsymbol{b}}}(t_i)\cdot\delta\boldsymbol{U}_i\right\rangle_{\overline{\Omega}}\tau_i + < \dot{\bar{\boldsymbol{t}}}(t_i)\cdot\delta\boldsymbol{U}_i >_{\overline{\Gamma}_t}\tau_i\,, \quad \forall\ \delta\boldsymbol{U}_i \in \overline{\mathcal{V}}_{\delta i}{}^{\mathrm{r}}\,. \tag{11b}$$

Here, the initial value is $\overline{\boldsymbol{u}}^{-}_i = \overline{\boldsymbol{u}}^{-}_{i-1} =: \boldsymbol{U}_{i-1}$ at time t^{-}_{i-1} and $\overline{\boldsymbol{u}}^{+}_{i-1} =: \boldsymbol{U}_i$ and $\delta\overline{\boldsymbol{u}}^{\mathrm{r}}_i = \delta\overline{\boldsymbol{u}}^{+}_{i-1} =: \delta\boldsymbol{U}_i$ compared to a downwind scheme.

3.2 Backwards-in-time and forwards-in-time methods of the dual problem

For numerical solution of the dual problem (6), we employ a temporally discretized version as for the primal problem in Subsection 3.1. To this end, we use the discontinuous approximations $\overline{\boldsymbol{u}}^{\mathrm{r}} \approx \overline{\boldsymbol{u}}^{\mathrm{r}}$, $\delta\overline{\boldsymbol{u}} \approx \delta\overline{\boldsymbol{u}}^{\mathrm{r}}$ and $\overline{\boldsymbol{z}} \approx \overline{\boldsymbol{z}}^{\mathrm{r}}$ such that Eq. (6) becomes with $\alpha = \varepsilon, \sigma$

$$\begin{aligned} \varrho_z(\overline{\boldsymbol{u}}^{\mathrm{r}}, \overline{\boldsymbol{z}}^{\mathrm{r}}; \delta\overline{\boldsymbol{u}}^{\mathrm{r}}) &= \mathrm{D}_{\overline{\boldsymbol{u}}^{\mathrm{r}}} \textstyle\sum_{i=1}^{N} \int_{I_i} Q_1(\overline{\boldsymbol{u}}^{\mathrm{r}}_i; \delta\overline{\boldsymbol{u}}^{\mathrm{r}})dt + \mathrm{D}_{\overline{\boldsymbol{u}}^{\mathrm{r}}(T)} Q_2(\overline{\boldsymbol{u}}^{\mathrm{r}}(T); \delta\overline{\boldsymbol{u}}^{\mathrm{r}}(T)) \\ &- \mathrm{D}_{\overline{\boldsymbol{u}}^{\mathrm{r}}} \textstyle\sum_{i=1}^{N} \underset{\sim}{\overline{B}}{}^{\alpha}_i(\overline{\boldsymbol{u}}^{\mathrm{r}}_i; \overline{\boldsymbol{z}}^{\mathrm{r}}_i, \delta\overline{\boldsymbol{u}}^{\mathrm{r}}) - \langle\delta\overline{\boldsymbol{u}}^{\mathrm{r}}(t_0), \overline{\boldsymbol{z}}^{\mathrm{r}}(t_0)\rangle \quad \forall\delta\overline{\boldsymbol{u}}^{\mathrm{r}} \in \overline{\mathcal{V}}_{\delta}{}^{\mathrm{r}}\,. \end{aligned} \tag{12}$$

The stress rate formulation $\overline{B}^{\sigma}_i(\overline{\boldsymbol{u}}^{\mathrm{r}}_i; \overline{\boldsymbol{z}}^{\mathrm{r}}_i, \delta\overline{\boldsymbol{u}}^{\mathrm{r}})$ requires a stress jump $[\overline{\boldsymbol{\sigma}}]$ and a strain jump $[\overline{\boldsymbol{\varepsilon}}(\overline{\boldsymbol{z}})]$ to obtain a temporal approximation of the dual problem. Consequently, using test and trial functions in Eq. (8) renders the bilinear forms in Eq. (12) as

$$\mathrm{D}_{\overline{\boldsymbol{u}}^{\mathrm{r}}} \sum_{i=1}^{N} \underset{\sim}{\overline{B}}{}^{[\sigma],\varepsilon(\overline{\boldsymbol{z}}),k}_i(\overline{\boldsymbol{u}}^{\mathrm{r}}_i; \overline{\boldsymbol{z}}^{\mathrm{r}}_i, \delta\overline{\boldsymbol{u}}^{\mathrm{r}}) = \mathrm{D}_{\overline{\boldsymbol{u}}^{\mathrm{r}}} \sum_{i=1}^{N} \int_{I_i} \left\langle \dot{\overline{\boldsymbol{\sigma}}}(\overline{\boldsymbol{u}}^{\mathrm{r}}_i) : \overline{\boldsymbol{\varepsilon}}(\overline{\boldsymbol{z}}^{\mathrm{r}}_i); \delta\overline{\boldsymbol{u}}^{\mathrm{r}} \right\rangle dt + \mathrm{D}_{\overline{\boldsymbol{u}}^{\mathrm{r}}} \sum_{i=1}^{N} \left\langle [\overline{\boldsymbol{\sigma}}(\overline{\boldsymbol{u}}^{\mathrm{r}}_i)]^k_j : (\overline{\boldsymbol{\varepsilon}}(\overline{\boldsymbol{z}}^{\mathrm{r}}_i))^-_j \right\rangle, \tag{13a}$$

$$\mathrm{D}_{\overline{\boldsymbol{u}}^{\mathrm{r}}} \sum_{i=1}^{N} \underset{\sim}{\overline{B}}{}^{\sigma,[\varepsilon(\overline{\boldsymbol{z}})],k}_i(\overline{\boldsymbol{u}}^{\mathrm{r}}_i; \overline{\boldsymbol{z}}^{\mathrm{r}}_i, \delta\overline{\boldsymbol{u}}^{\mathrm{r}}) = \mathrm{D}_{\overline{\boldsymbol{u}}^{\mathrm{r}}} \sum_{i=1}^{N} \int_{I_i} \left\langle \dot{\overline{\boldsymbol{\sigma}}}(\overline{\boldsymbol{u}}^{\mathrm{r}}_i) : \overline{\boldsymbol{\varepsilon}}(\overline{\boldsymbol{z}}^{\mathrm{r}}_i); \delta\overline{\boldsymbol{u}}^{\mathrm{r}} \right\rangle dt + \mathrm{D}_{\overline{\boldsymbol{u}}^{\mathrm{r}}} \sum_{i=1}^{N} \left\langle (\overline{\boldsymbol{\sigma}}(\overline{\boldsymbol{u}}^{\mathrm{r}}_i))_j : [\overline{\boldsymbol{\varepsilon}}(\overline{\boldsymbol{z}}^{\mathrm{r}}_i)]^{-,k}_j \right\rangle, \tag{13b}$$

and where $j = i+1$ for $k = d$ and $j = i-1$ for $k = u$. In [7], it is shown that eight approximations of the dual problem are obtained when the strain rate formulation $\overline{B}^{\dot{\varepsilon}}_i(\overline{\boldsymbol{u}}^{\mathrm{r}}_i; \overline{\boldsymbol{z}}^{\mathrm{r}}_i, \delta\overline{\boldsymbol{u}}^{\mathrm{r}})$ is considered. In Eq. (13a), we consider a dependency of the jump terms $[\sigma]$ on the functions $\overline{\boldsymbol{u}}^{\mathrm{r}}_i, \overline{\boldsymbol{u}}^{\mathrm{r}}_j$. Consequently, a localization for each time increment I_i of the dual residual $\varrho_z(\overline{\boldsymbol{u}}^{\mathrm{r}}, \overline{\boldsymbol{z}}^{\mathrm{r}}; \delta\overline{\boldsymbol{u}}^{\mathrm{r}})$ in Eq. (12) is not possible, as for the primal residual $\overline{\rho}$ in Eq. (3a).

We recall $\overline{\boldsymbol{u}}^{\mathrm{r}}_i(t) = \overline{\boldsymbol{u}}^{+}_{i-1} =: \boldsymbol{U}_i = \text{const}, \quad \delta\overline{\boldsymbol{u}}^{\mathrm{r}}_i(t) = \delta\overline{\boldsymbol{u}}^{\mathrm{r}}_i =: \delta\boldsymbol{U}_i = \text{const}, \quad t \in I_i$ and, moreover, $\overline{\boldsymbol{z}}^{\mathrm{r}}_i(t) = \overline{\boldsymbol{z}}^{+}_{i-1} =: \boldsymbol{Z}_i = \text{const}$. Consequently, the discretized dual problem Eq. (12) becomes

$$\begin{aligned} \varrho_z(\boldsymbol{U}, \boldsymbol{Z}; \delta\boldsymbol{U}) &= -\textstyle\sum_{i=1}^{N} \mathrm{D}_{\boldsymbol{U}_i} Q_1(\boldsymbol{U}_i; \delta\boldsymbol{U}_i)\tau_i - \mathrm{D}_{\boldsymbol{U}_N} Q_2(\boldsymbol{U}_N; \delta\boldsymbol{U}_N) - \langle\delta\boldsymbol{U}(t_0), \boldsymbol{Z}(t_0)\rangle \\ &- \mathrm{D}_{\boldsymbol{U}} \textstyle\sum_{i=1}^{N} \langle(\overline{\boldsymbol{\sigma}}_i(\boldsymbol{U}_i) - \overline{\boldsymbol{\sigma}}_{i-1}(\boldsymbol{U}_{i-1})) : \overline{\boldsymbol{\varepsilon}}_i(\boldsymbol{Z}_i); \delta\boldsymbol{U}_i\rangle = 0 \qquad \forall\ \delta\boldsymbol{U}_i,\ i = 0, ..., N. \end{aligned} \tag{14}$$

Eq. (14) indicates a backwards-in-time problem, due to the terms related to the i+1st time step. Compared to Eq. (13a), Eq. (13b) presents a dependency of jump terms $[\varepsilon(\overline{\boldsymbol{z}})]$ on the functions $\overline{\boldsymbol{z}}^{\mathrm{r}}_i, \overline{\boldsymbol{z}}^{\mathrm{r}}_j$. Exploiting the property $\delta\overline{\boldsymbol{u}}^{\mathrm{r}}_i|_{\notin I_i} = \boldsymbol{0}$ in Eq. (8c) for the test functions $\delta\overline{\boldsymbol{u}}^{\mathrm{r}} \in \overline{\mathcal{V}}_{\delta}{}^{\mathrm{r}}$, the dual residual $\varrho_z(\overline{\boldsymbol{u}}^{\mathrm{r}}, \overline{\boldsymbol{z}}^{\mathrm{r}}; \delta\overline{\boldsymbol{u}}^{\mathrm{r}})$ in Eq. (12) can be localized, and can be solved by a time-stepping scheme. $\overline{\boldsymbol{z}}^{-}_{i-1}$ denotes the initial value at time t^{-}_{i-1}. Then setting $\mathrm{r} = 0$

Table 1: Summary of material parameters.

	E [MPa]	ν [−]	c [−]	Y_0 [MPa]	H_1 [MPa]	q [−]	b [−]	H_2 [MPa]	m [−]
Inclusion	400000	0.2	0.1	−	−	−	−	−	−
Matrix	76500	0.3	−	200	300	111	608.5	300	1

in (8c) with regard to trial and test functions $\overline{\boldsymbol{z}}_i^{\mathrm{r}}(t) = \overline{\boldsymbol{z}}_i{}^{-} = \overline{\boldsymbol{z}}_{i-1}^{+} =: \boldsymbol{Z}_i = \text{const}, \overline{\boldsymbol{z}}_{i-1}^{\mathrm{r}}(t) = \overline{\boldsymbol{z}}_{i-1}^{-} =: \boldsymbol{Z}_{i-1}, \overline{\boldsymbol{u}}_i^{\mathrm{r}}(t) = \overline{\boldsymbol{u}}_i^{+} = \overline{\boldsymbol{u}}_{i-1}^{+} =: \boldsymbol{U}_i = \text{const}, \delta\overline{\boldsymbol{u}}_i^{\mathrm{r}}(t) = \delta\overline{\boldsymbol{u}}_i^{\mathrm{r}} =: \delta\boldsymbol{U}_i = \text{const}, t \in I_i$, $\dot{\overline{\boldsymbol{\varepsilon}}}(\overline{\boldsymbol{u}}^{\mathrm{r}}) = \nabla^{\mathrm{sym}}\dot{\overline{\boldsymbol{u}}} = \boldsymbol{0}$, $\dot{\overline{\boldsymbol{\sigma}}}(\overline{\boldsymbol{X}}) = \boldsymbol{0}$ such that $\int_{I_i} \left\langle \dot{\overline{\boldsymbol{\sigma}}}(\overline{\boldsymbol{u}}_i^{\mathrm{r}}) \colon \overline{\boldsymbol{\varepsilon}}[\overline{\boldsymbol{z}}_i^{\mathrm{r}}] \right\rangle dt = 0$, the discretized dual problem Eq. (12) renders

$$\begin{aligned} \varrho_z(\boldsymbol{U}, \boldsymbol{Z}; \delta\boldsymbol{U}) \;&=\; \textstyle\sum_{i=1}^{N} \mathrm{D}_{\boldsymbol{U}_i} Q_1(\boldsymbol{U}_i; \delta\boldsymbol{U}_i)\tau_i + \mathrm{D}_{\boldsymbol{U}_N} Q_2(\boldsymbol{U}_N; \delta\boldsymbol{U}_N) - \langle \delta\boldsymbol{U}(t_0), \boldsymbol{Z}(t_0)\rangle \\ &-\; \mathrm{D}_{\boldsymbol{U}_i} \textstyle\sum_{i=1}^{N} \left\langle \overline{\boldsymbol{\sigma}}_i(\boldsymbol{U}_i) : (\overline{\boldsymbol{\varepsilon}}_i(\boldsymbol{Z}_i) - \overline{\boldsymbol{\varepsilon}}_{i-1}(\boldsymbol{Z}_{i-1})) \,; \delta\boldsymbol{U}_i \right\rangle = 0 \qquad \forall\ \delta\boldsymbol{U}_i,\ i = 0, ..., N. \end{aligned} \tag{15}$$

In contrast to Eq. (14), Eq. (15) indicates a forwards-in-time problem since no terms related to the $i+1$st time step are involved. For an effective study of the proposed adaptive approach, an accurate estimate of the exact global error E^{j} is introduced as viewed in [8], called the *actual* error $\hat{E}^{\mathrm{j}}$.

4 NUMERICAL EXAMPLE

A compact tension (CT) specimen is investigated. Due to symmetry properties, a half model is considered as illustrated in Fig. 1a. The initial mesh discretization is shown in Fig. 1b. A plane strain state is assumed. The specimen is stretched by a displacement $\overline{u}^* = 0.08$ mm in the vertical direction, which is uniformly distributed on the entire boundary of the hole. The quantity of interest in Eq. (5) is defined as the following local type quantity

$$Q := \int_I \int_{\overline{\Omega}'} \overline{\sigma}_{22}(\overline{u}) dv dt + \int_{\overline{\Omega}'} \overline{\sigma}_{22}(\overline{u}_T) dv, \tag{16}$$

where $\overline{\sigma}_{22}$ represents a component of the macro stress tensor $\overline{\boldsymbol{\sigma}}$. $\overline{\Omega}'$ is the local green domain in Fig. 1a, with $r = 4$ mm. The CT-specimen is assumed to be homogeneous on the macro-scale. But it is inhomogeneous on the micro-scale as its microstructure is composed of a periodic distributed composite material which consists of an inclusion and a matrix as illustrated in Fig. 1c. For the inelastic micro constituent, the classical von Mises plasticity is assumed. The matrix is an aluminum alloy with elasto-plastic properties characterized by nonlinear isotropic hardening and linear kinematic hardening, while all inclusion fibers are ceramic with linear elastic properties. The material parameters and the volume fraction of inclusion c are shown in Tab. 1. A total number of 100 time steps are used during each mesh adaptivity step. The model hierarchy, which provides a balance between the accuracy and the numerical efficiency of homogenization methods, is based on the basic mean-field model self-consistent, the mean-field interaction direct derivative and the full-field FEM under periodic boundary condition with hierarchical order (n = 0), (n = 1) and (n > 1), respectively. As displayed in Figs. 2a and 2b for the forwards-in-time method, the local mesh refinements are initially concentrated within the local

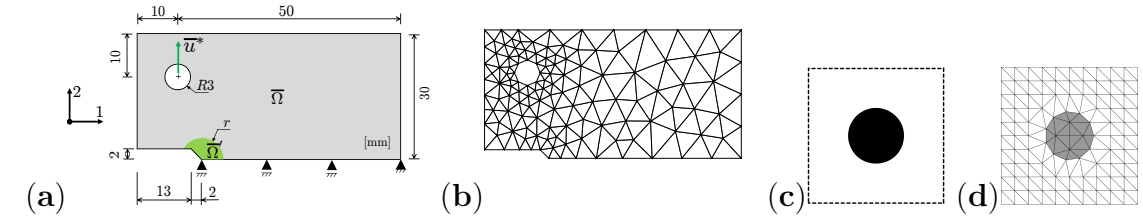

Figure 1: Geometry and boundary conditions of CT specimen under tension (**a**); Initial mesh of CT specimen (**b**); Representative volume element (**c**) and its mesh (**d**)

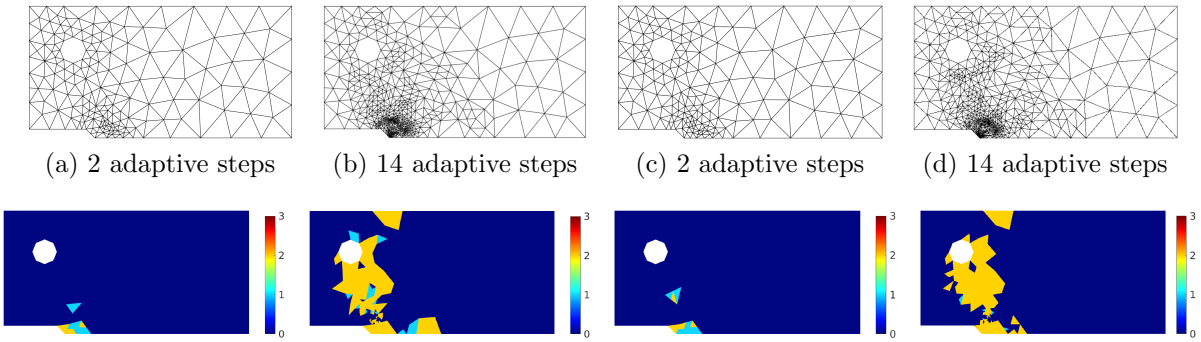

(a) 2 adaptive steps (b) 14 adaptive steps (c) 2 adaptive steps (d) 14 adaptive steps

(e) 2 adaptive steps (f) 14 adaptive steps (g) 2 adaptive steps (h) 14 adaptive steps

Figure 2: CT specimen under tension: Adaptivity refined distribution; forwards-in-time method (**a**-**b**), backwards-in-time method (**c**-**d**): Adaptivity refined model distribution; forwards-in-time method (**e**-**f**), backwards-in-time method (**g**-**h**)

domain $\overline{\Omega}'$ in the quantify of interest Eq. (16) before spreading to nearby areas. These mesh refinements are also observed for the backwards-in-time method as shown in Figs. 2c and 2d. The resulting model distributions are depicted in Figs. 2e-2f and in Figs 2g-2h with the forwards-in-time method and backwards-in-time method, respectively. Figs. 2f and 2h show that computational expensive full-field methods are more used during model adaptivity with backwards-in-time method compared with forwards-in-time method. Fig. 3 illustrates the quantity of interest $Q_{\mathrm{h}}^{(\mathrm{n}),(\mathrm{j})}$, the relative actual error $\hat{E}_{\mathrm{rel}}^{\mathrm{j}}$, and the relative error estimate $\tilde{E}_{\mathrm{rel}}^{\mathrm{j}}$ over each adaptive step j. Fig. 3a presents a convergence of the quantity of interest $Q_{\mathrm{h}}^{(\mathrm{n}),(\mathrm{j})}$ to the reference value Q_{ref} while Fig. 3b shows that the relative actual error $\hat{E}_{\mathrm{rel}}^{\mathrm{j}}$ is already reduced significantly and effectively after 14 adaptive steps. Furthermore, with regard to Fig. 3 the results obtained with the forwards-in-time method are quite similar to the result obtained with the backwards-in-time method.

5 CONCLUSIONS

To sum up, the proposed framework of goal-oriented adaptivity takes into account accumulation over the time of discretization error due to the mesh and elasto-plastic homogenization model. Therefore, forwards-in-time and backwards-in-time methods are developed to solve the dual problem. However, the forwards-in-time method is more effective than the backwards-in-time method as it does not need additional memory capacity to store the primary solutions computed over all time steps. In addition, the primal

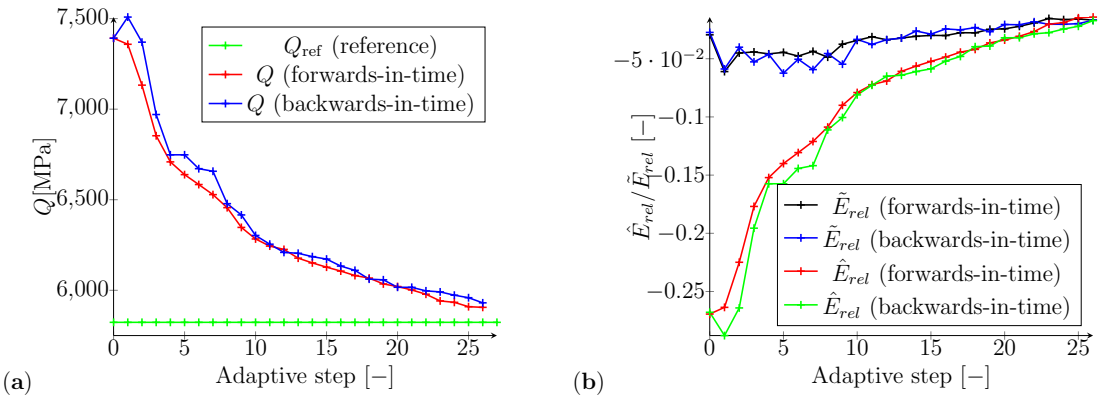

Figure 3: CT specimen under tension: Mesh and model adaptivity : Quantities of interest (**a**), relative actual error $\hat{E}_{rel}$ and relative error estimate $\tilde{E}_{rel}$(**b**)

problem is solved either with an explicit Euler forwards time interaction scheme using a downwind approximation or with an implicit Euler backwards time interaction scheme using an upwind approximation.

REFERENCES

[1] R. Mahnken, "New low order Runge-Kutta schemes for asymptotically exact global error estimation of embedded methods without order reduction", *Comp. Methods Appl. Mech. Engrg.*, Vol. **401**, Art. no. 115553, (2022).

[2] G. Thomas Masse, R. E. Smelser, and J. S. Rossmann, *Continuum Mechanics for Engineers* CRC Press, Boca Raton (2020).

[3] R. Mahnken and X. Ju, "Goal-oriented adaptivity based on a model hierarchy of mean-field and full-field homogenization methods in linear elasticity", *Int. J. Numer. Meth. Engng.*, Vol. **00**, pp. 1-36, (2019).

[4] R. Hill, "Elastic properties of reinforced solids: some theoretical principles". *J. Mech. and Phys. Solids.* , 357–372, (1963).

[5] M. Schmich, B. Vexler, "Adaptivy with dynamic meshes for space-time finite element discretizations of parabolic equations". *SIAM* **30**, pp. 369-393, (2008).

[6] K. Eriksson, D. Estep, P. Hansbo, and C. Johnson, *Introduction to Adaptive Methods for Differential Equations*. Acta Numerica, (1995).

[7] R. Mahnken, A. T. Simeu "Downwind and upwind approximations for primal and dual problems of elasto-plasticity with Prandtl-Reuss type material laws". *in preparation*, (2023).

[8] A. T. Simeu, R. Mahnken, "Goal-oriented adaptivity based on a model hierarchy of mean-field and full-field homogenization methods in elasto-plasticity". *PAMM* **22**, (2022).